Heating rate effect on the moisture clog while drying refractory castables - A neutron tomography perspective

M. H. Moreira[a,*], S. Dal Pont[b], A. Tengattini[b,c], V. C. Pandolfelli[a]

[a] *Federal University of Sao Carlos, Graduate Program in Materials Science and Engineering (PPGCEM), Rod. Washington Luiz, km 235, 13565-905, São Carlos, SP, Brazil*

[b] *Université Grenoble Alpes, CNRS, Grenoble INP, 3SR, 38000 Grenoble, France*

[c] *Institut Laue Langevin, 71 Avenue des Martyrs, 38000 Grenoble, France*

Abstract

Due to their great performance and ease of installation, refractory castables are common ground materials to enable high temperature processes. However, their fully operational condition is slowed down by the gradual drying stage required. Therefore, better understanding of the moisture transport involved is essential to improve their efficiency and reduce the likelihood of explosive spalling events due to vapor pressurization. Neutron tomography provides a relevant inner view of the moisture distribution across a sample and its evolution over time. In this work, the effect of the heating rate on moisture clog was investigated and compared with available laboratory and industrial observations. It was found out that higher heating rates resulted in a faster and longer lasting water accumulation ahead of the drying front, in agreement with other macroscopic studies and explaining the common reasoning behind using slower heating rates and safer industrial operations.

*Corresponding Author

Email address: murilo.moreira@estudante.ufscar.br (M. H. Moreira)

This study highlights the potential of neutron imaging for the ongoing effort to maximize the efficiency of refractory castables drying process by controlling the moisture accumulation without exclusively relying on slower heating rates.
Keywords: Refractory Castable, Neutron Tomography, Drying, High Temperature

---

1. Introduction

Steel and cement are two of the most consumed building materials in the world [1]. For their production, several necessary transformations occur at high temperatures and to safely and efficiently ensure the required processing demands ranging from high temperatures to mechanical stresses and chemical attacks, refractory materials are irreplaceable [2, 3].

The class of monolithic refractories differs itself from its alternatives because it can be cast *in-situ* into its final shape [2, 3]. This speeds up the application procedure, decreasing the maintenance time of the industrial equipment. To attain the rheological features that enable such a behavior, water is commonly added to produce a raw material suspension. For hydraulically bonded refractories, the water also reacts with the binders, resulting in crystalline precipitates that increase the mechanical strength of the green body during the curing stage [2].

The demand for improved efficiency yielded materials with increased mechanical strength and corrosion resistance, although reducing their porosity at the green state [4]. This, in turn, requires slower heating during the drying step to prevent explosive spalling of the refractory lining [3, 4], which

has become the most challenging technical limitation. This considerably reduces the benefits of hydraulic bonded monolithics, increasing costs due to the slower processing, higher energy consumption associated to the lower heating rate and also to the greater carbon footprint [5].

Consequently, explosive spalling is a key topic as its first observation in concrete structures is subjected to fire [6]. The most accepted explanation of this phenomenon is the superposition between thermomechanical stresses and water pressurization inside the material pores [6, 7, 8]. A key phenomenon in spalling is moisture clogging when water evaporates in the warmer regions and condensates in the colder ones, decreasing the effective permeability. This pressurizes the water vapor, which can generate cracks, damaging the structure.

Interest regarding the drying behavior of refractories is also driven by the potential reduction of the economical and environmental costs associated to the monolithics processing. Studies ranged from laboratory scale thermogravimetric tests (TGA) [9, 10, 11] to those based on pressure and temperature sensors [12, 13, 14], or even more advanced techniques, such as nuclear magnetic resonance (NMR) [15, 16] and neutron tomography [17].

Full-field techniques, such as neutron imaging describe the entirety of a sample and the evolving water distribution within it, rather than providing macroscopic or point-wise information as the other techniques. Additionally, non-destructive techniques do not affect the sample, as they do not require sensors placed within them. This is especially important, as it was observed that the presence of even very thin thermocouples can trap air bubbles at their interfaces, affecting the local microstructure and possibly interfering

with the readings of such devices highlighting the scattering range of pressure values obtained when using such techniques [18, 19].

The most common imaging approaches generally applied to Portland cement concrete are neutron and X-ray tomography, and Nuclear Magnetic Resonance (NMR), [20, 18, 21, 22]. The two former differ in terms of the nature of the ionizing beam used and its physical interaction with the sample and the water. Notably, X-rays have less interaction with water, yielding a lower contrast, making the post-treatment stages more challenging and the final result more prone to numerical artifacts. For more details, the reader is referenced to the review on the experimental techniques to assess water removal by Luz et al. [4]. NMR quantifies instead the relaxation time of the water molecules, detecting the water content and its configuration inside the sample [21]. However, this technique does not yield a 3D representation of the water distribution at high resolutions and most importantly, it is not fast enough to capture the dynamics of drying, something that tomography based techniques are capable of.

One of the key control parameters of the refractory castable drying process is the heating rate. It is well known that faster temperature increases lead to a greater likelihood of explosive spalling as shown by TGA analysis [3, 23, 10]. However, the effect of the heating rate on the water distribution within the sample itself is still unknown as the available studies tackle the macroscopic response of the sample instead of its full-field response provided by imaging tests, such as the neutron tomography setup used by Moreira et al. [17]. Additionally, the most common technique applied for studying these effects, the TGA, generates a thermal gradient that is not representative of

unidirectional heating attained when drying refractory linings in industrial applications, as schematically shown in Figure 1 (a). The unidirectional heating of the sample via the neutron tomography setup is shown in Figure 1 (b).

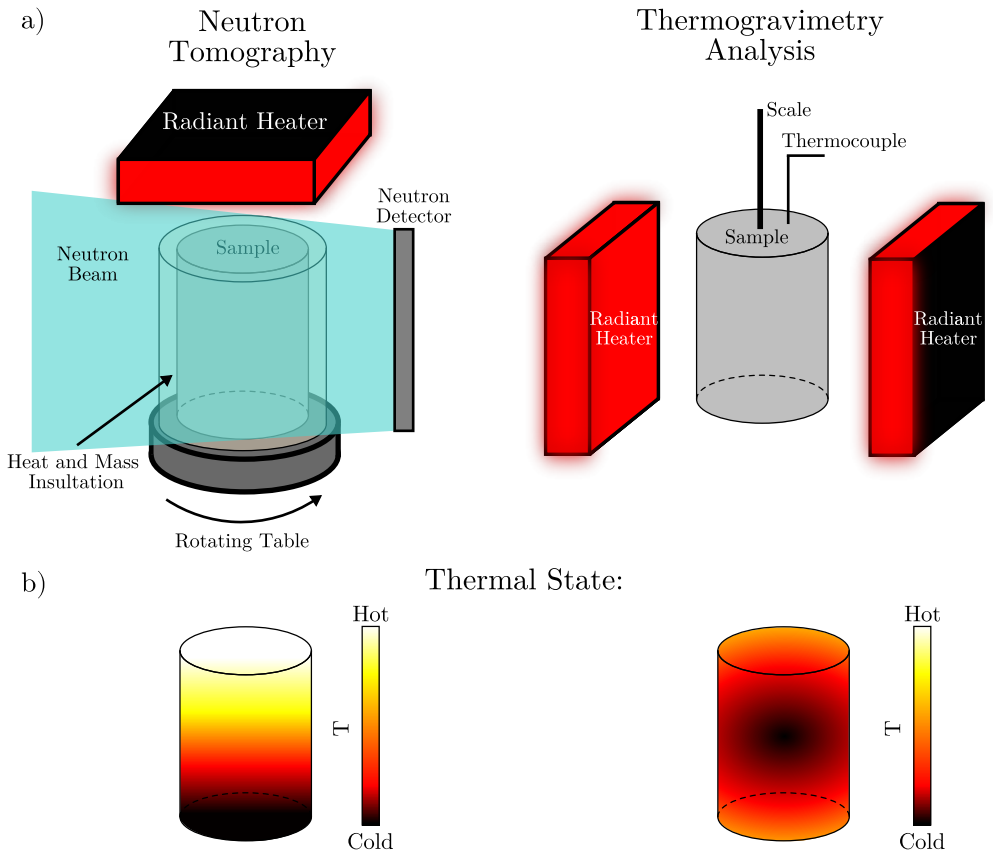

Figure 1: Differences between a general thermogravimetry analysis (a) and the neutron tomography setup (b) used by Moreira et al. [17] and the resulting thermal state of the samples. The neutron tomography setup provides a one-directional gradient whereas the TGA for small samples results only in a minor radial temperature distribution.

For the neutron tomography experiments, the radiant heater is placed at

the top of the cylindrical sample and the radial sides are insulated, inducing an unidimensional thermal energy and moisture transport phenomena, which results in a linear and steep thermal gradient. For the TGA test, the heating elements are placed at the lateral sides of the sample and all surfaces are free to exchange heat and mass. This leads to a smaller, radially distributed thermal gradient. The interpretation of the effect of the drying rate on the moisture clog position and intensity is then more cumbersome.

Applying a similar setup than the one shown in Figure 1 (b), but based on NMR, Barakat et al. suggested an in-depth analysis of the heating rate effect on the dynamics of water removal from refractory monolithics for future research [24]. The heating rate applied during the drying of calcium aluminate cement high-alumina castables analyzed in their study was in the range of 1-2°C/minute.

Barakat et al. reported preliminary results using a lower heating rate, 0.3°C/min-0.4°C/min, for the NMR tests and found out that the drying front position followed, in both cases, a linear function of time. Moreover, there was a minor increase in the drying front velocity for higher heating rates, whereas the front temperature was virtually the same, as shown in Figure 2.

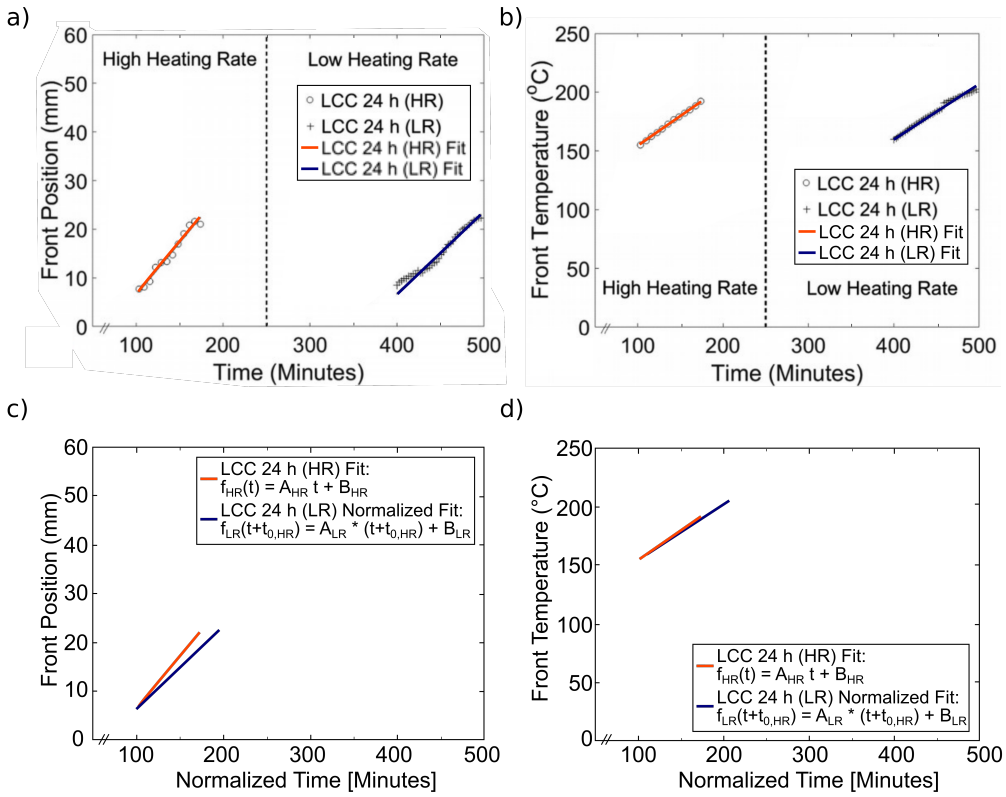

Figure 2: Heating rate effect analyzed by Barakat et al. [24], considering the front position (a) and the front temperature (b). The linear fits were shifted in time to enable an easier comparison in (c) and (d). LCC stands for low cement castable

The first experimental evidence of the moisture clog phenomenon using the neutron tomography was reported by Dauti et al. [20], and later conclusively proven by Moreira et al. [17]. In the current work, the effect of the heating rate on the moisture transport while drying the calcium aluminate cement refractory castable is studied by neutron tomography and the results attained are compared with those in the literature. These findings have clear implications with the industrial demands and highlight the potential of the

approach adopted here for improving the efficiency of the drying processes in monolithic refractories.

2. Material and Methods

2.1. Refractory Castable Composition and Processing

A calcium aluminate cement high-alumina vibratable castable was prepared following the Andreasen particle packing model with $q = 0.21$. The final composition can be found in Table 1. The refractory composition was homogenized for 1 min and mixed with water for an additional 3 min in a paddle mixer equipped with a torquemeter [25]. The composition was then cast into a cylindrical mullite and alumina ceramic casings (50mm in height and 33mm in diameter) - it was found in preliminary studies that both mullite and alumina presented the same performance in avoiding the mass transport in the radial direction. The curing step for the castable within the case was at 30°C under 80% of relative humidity in a climate chamber for 24h.

The use of fine aggregates (AT 1-0.5 and smaller, $<$ 1mm) in the final refractory composition is challenging for rapid neutron tomography, given that the true resolution in sub-minute tomographies is larger than these particles [20, 18, 17]. This can lead to difficulties when accurately calculating the volume fractions of the components (aggregates, dry and wet cement paste, and pores). Nevertheless, fine aggregates are important for castables commonly applied as refractory linings, which is why they were kept in the formulation. It should be noted, however, that to accurately quantify each phase (matrix, pores, water and aggregates), a smaller spatial resolution would be needed.

Table 1: High-alumina refractory castable composition.

Raw materials		Compositions (wt.%)
Tabular alumina	AT 6-3 (Almatis, Germany)	18
	AT 3-1 (Almatis, Germany)	10
	AT 1-0.5 (Almatis, Germany)	11
	AT 0.6-0.2 (Almatis, Germany)	9
	AT 0.2-0 (Almatis, Germany)	16
	AT < 45 (Almatis, Germany)	10
Calcined and reactive alumina	CL370 (Almatis, Germany)	11
	CT3000SG (Almatis, Germany)	10
Calcium Aluminate Cement	Secar 71 (Imerys Aluminate, France)	5
Water	Distilled water	4.5
Dispersant	Castament FS60 (BASF, Germany)	0.2
Free-flow	(%)	75

2.2. Samples and Experiment Layout

The unidirectionality of the heat and mass transport is important to keep the boundary conditions reproducible and close to the industrial applications conditions and also to simplify the quantification of moisture transport from the resulting images [20, 18, 17]. This was attained by using mullite and alumina ceramic casings. These materials were selected because they are transparent to the neutron beam, impermeable to water vapor, and mostly important, presenting a lower thermal expansion than the refractory castable. This prevents radial mass transport even at higher temperatures [17].

The neutron tomography tests were conducted on the NeXT instrument at the Institut Laue-Lavengin (ILL) [26], adopting the same imaging condi-

tions as in [18, 17]. A tomography was acquired every 58.5s and the true spatial resolution of each tomography was of 160 μm. The heating was achieved using an infrared radiator heater (Elstein HTS - High Temperature Heater, Germany) placed parallel to the top surface of the cylinder sample. Two different heating conditions were tested, i) a faster heating, with a rate of roughly 158°C/min up to a temperature of 500°C (as the ones used by Dauti and Tengattini et al. [20, 18]) and (ii) a slower heating rate of 10°C/min, as proposed by Moreira et al. [17]. Both conditions are outlined in Figure 3.

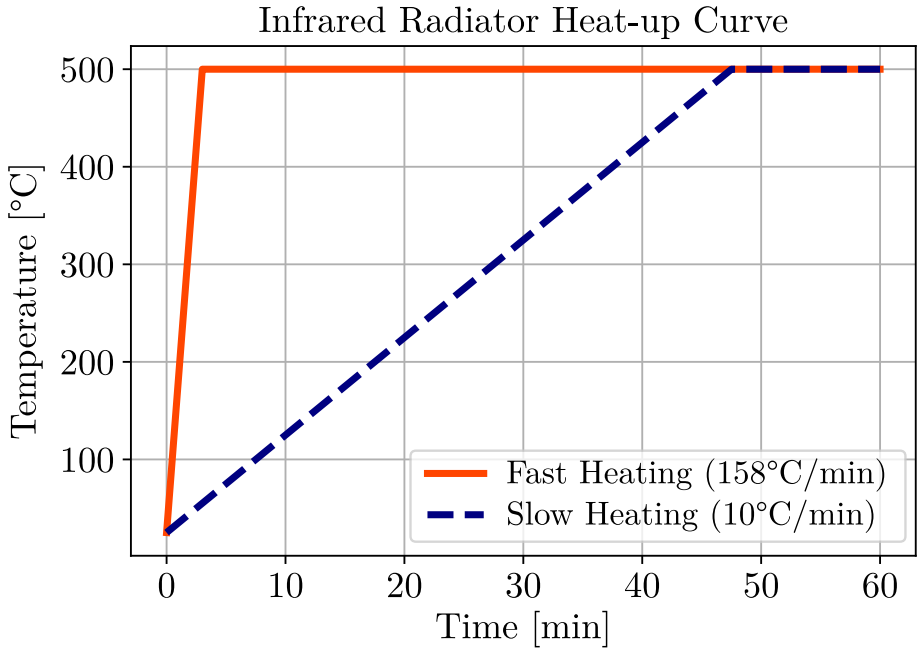

Figure 3: Heating rates used during the neutron tomography drying tests.

2.3. Image analysis

The tomographies obtained by using the NeXT equipment were reconstructed through the filtered back projection algorithm implemented by the

commercial software X-act (from RX Solutions, France).

The aggregates are, at the first approximation, an impermeable phase [27], whose main contribution to drying is played by the Interfacial Transition Zone, ITZ, the layer around the grains where the higher porosity enhances the mass transport [28]. In the current image analysis, the aggregates were therefore withdrawn, after isolating them with a gray value-based threshold segmentation, applied over the median of the first ten tomographies as described by Moreira et al. [17].

The position of the drying front is obtained by locating it on the sudden change of attenuation caused by the water migration, corresponding to a minimum in the gray value gradient along the axial direction. To reduce the noise, this is calculated over the average of a cylinder slice of the sample, under the assumption of uniaxiality of the drying front. To further reduce the noise, the Savitzky-Golay [29] digital filter was applied to the intensity values. More details about this procedure can be found in [17].

To detect moisture accumulation, the relative changes of intensity with respect to the initial state $\psi(t)$ were analyzed, and specifically the median intensity of the first ten tomographies as detailed in Equation 1:

$$\psi(t) = \frac{\left(I(\mathbf{x},t) - \hat{I}(\mathbf{x},t_0)\right)}{\hat{I}(\mathbf{x},t_0)} \times 100\% \tag{1}$$

where, $\hat{I}(\mathbf{x},t_0)$ is the median intensity dataset of the first ten tomographies.

3. Results and Discussions

The effectiveness of the drying process in industrial applications is driven by the temperature increase on the hot surface of the refractory lining [3, 30,

31]. The evolution of such temperatures over time is generally known as the heat-up curve. The current section compares the effect of two heating rates (fast heating - 158°C/min and slow heating - 10°C/min, as imposed by the infrared heater) on refractory castable samples. Figure 4 shows the relative changes in the water distribution for the two rates.

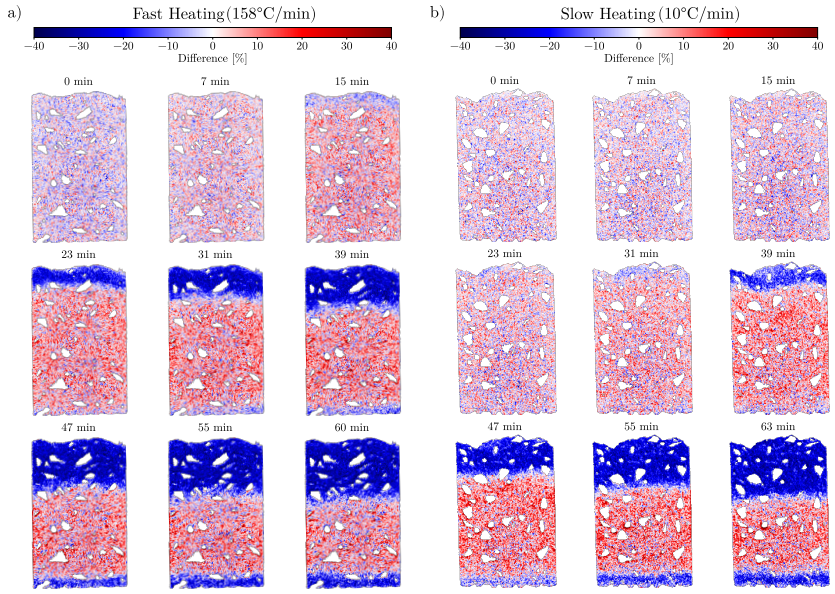

Figure 4: Relative changes in water distribution for the fast and slow heating conditions.

After 15 minutes (or less), a drying front was detected at the top of the sample under the fast heating condition. The equivalent drying stage was reached after 31 minutes for the slow condition. Another important observation is the quick increase of water content ahead of the front for the former.

After moving inwards, in the time range between 23 and 47 minutes, the front starts to slow down for the fast heating case. The final stages of both heating conditions are instead practically indistinguishable.

Figure 5 is a contour plot of the temporal evolution of the moisture content difference based on its initial moisture condition (reference state). Each point represents the average at a given depth. The two level curves corresponding to relative differences of 0% and 5% are marked to highlight the drying front and the moisture accumulation zone, respectively. In both maps, the level curves for fast (in dotted black) and slow (yellow) heating conditions, are shown to simplify the comparison.

This highlights that water accumulation already initiates after 10min for the fast heating sample spanning from the positions 40mm to 45mm (5mm to 10mm away from the heated surface - henceforth referred to as top). Within 20 minutes, the increase in attenuation higher than 5% reaches the 35mm point. This suggests that higher heating rates induce moisture accumulation closer to the hot surface and earlier.

Figure 5 (b) highlights how under slow heating conditions moisture accumulation initiates later, evolves slowly, most likely reducing the permeability at a correspondingly slower rate. These observations agree with TGA results [23] and industrial observations [30] that suggest a direct relation between the heating rate and the likelihood of explosive spalling.

To simplify the quantitative comparison, Figure 6 reports the normalized gray value evolution throughout time, averaged over specific heights of the sample.

The fast heating sample showed evident moisture accumulation (marked by a normalized average gray value higher than 1) across the sample, which quickly starts to develop after 5 minutes. The slow heating sample showed instead negligible moisture accumulation between the 1.6mm and 39.7mm

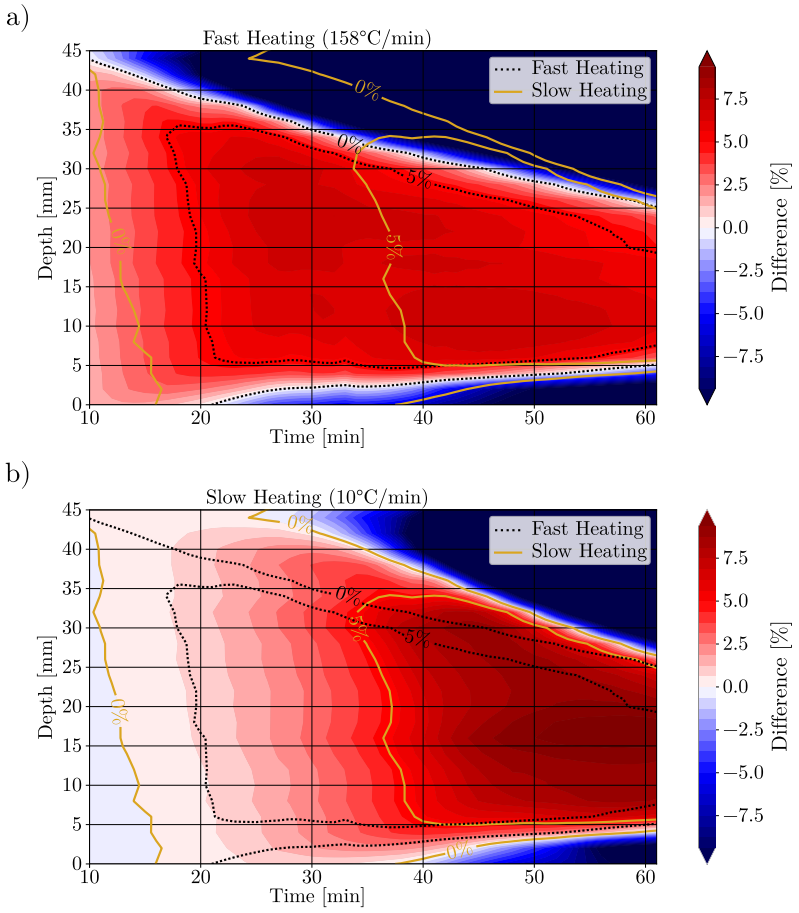

Figure 5: Average on the radial direction of the water difference distribution as a function of time for the samples dried under fast and slow heating protocols (a) and (b). The heater is placed towards the top of the sample at the 45mm mark. The results were averaged over slices of 2mm thickness in the axial direction. The contours with relative differences equal to 0% and 5% are highlighted as black dotted lines for fast heating and dark yellow for the slow heating tests. Higher values of difference (dark red) indicate water accumulation, whereas lower values (dark blue) represent drying. The results of the first ten tomographies (the first 10 minutes of the test) are not described here, as they are the reference state.

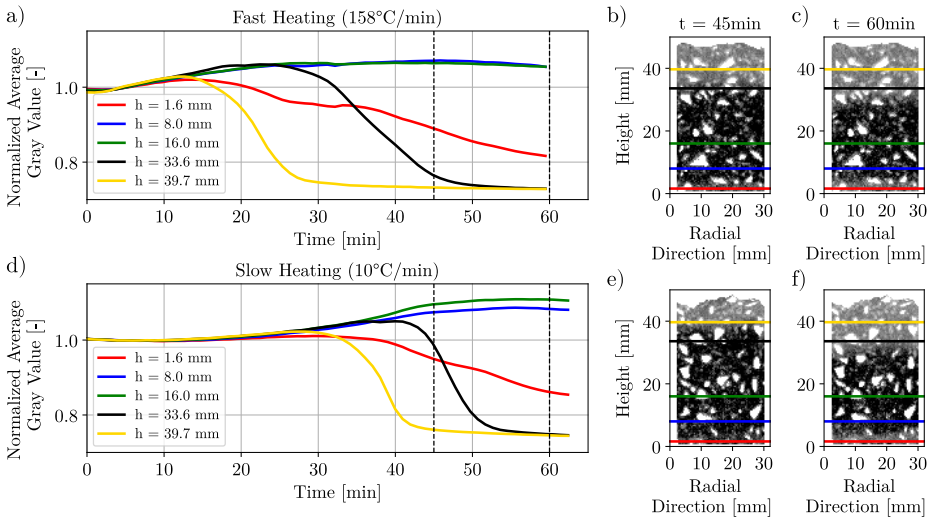

Figure 6: Normalized average gray value evolution at specific heights of the sample for (a) fast heating condition and (d) slow heating one. Representative vertical slices of the tomographies at 45 and 60 minutes, marking the positions corresponding to the plots for fast heating - (b) and (c) -, and slow heating - (e) and (f) are presented.

depth region. Under such a condition it takes longer to be developed (starting after 25 min), but affects a larger portion of the sample. On the other hand, the time length for which the water accumulation is detected is shorter, especially when comparing the time taken for the position 33.6mm to reach values higher than 1 (around 25 minutes for the slow condition and roughly 3 minutes for the fast one).

The highest moisture accumulation zone also shifts, peaking at 16mm for the slower case, and spanning the region between 8 and 16mm for the faster one. This attests the observations in Figure 5.

These observations agree with the macroscopic and empirical ones. For instance, Portland cement structures under fire (thus, very high heating rates) are usually damaged in successive removals of layers [6], whereas refractory castables heated at a much slower rate, can undergo explosive spalling of thick layers, that are thrust several meters away [30].

Other key factors may induce this different behavior. Portland cement concrete components are usually shaped with reinforcement bars in their structure, and the dehydration reactions differ between the hydrated phases of calcium silicate (Portland cement) and calcium aluminate (refractory castables) [32]. Further studies exploring the heating rate effects on explosive spalling of both classes of materials seems, nonetheless, of great importance.

Figure 7 reports the mean relative difference of attenuation and its time derivative over 12 voxel thick disks (to minimize noise) at the top the samples. It is worth noting that positive derivatives indicate a water content increase, while negative derivatives, a decrease. This highlights areas of rapid variation of the drying speed; for example the fast heating sample shows an early

increase of water content at the beginning of the test in the region of interest, followed by negative peaks that appear after 12 min and 22 min. After 30 minutes, the drying rate decreases and stabilizes to roughly -0.16°C %/min. A linear fit with a coefficient of determination of 0.99 confirms this in Figure 7.

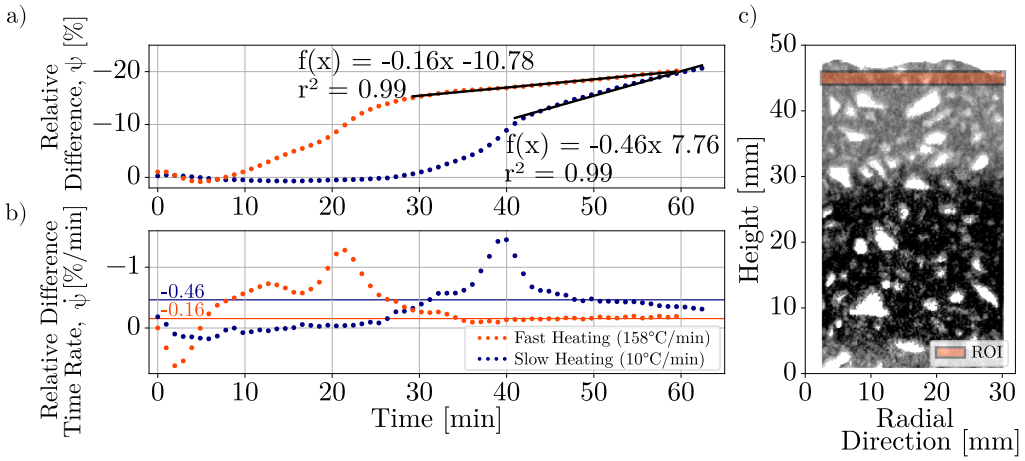

Figure 7: Relative difference evolution of a 2mm slab at the top of the samples (a) and the relative difference time rate (b). The axial slice presented in (c) is only to highlight the region of interest.

The slow heating sample warms slowly for the first 23 minutes, when an initial increase in moisture is detected, followed by a short plateau and a peak after 40 minutes, followed by a decrease. At the end of the test, the drying rate is close to -0.46 %/min, almost 3 times higher than the fast heating case. This rate appears to slow down and would likely reach the same plateau as the fast heating sample.

When considering these differences in the drying rate, the dehydration reactions are critical to understanding the observed differences. The drying

rate peak positions and intensities observed could be related to the kinetics of dehydration which are sensitive to the heating rate. Figure 8 (a) shows the thermogravimetric analysis for different samples with the same chemical composition studied herein at heating rates of 2°C/min, 5°C/min and 20°C/min. It shows how drying (decrease of mass) is shifted to higher temperatures at higher heating rates - comparing the TGA % in Figure 8 (a) at 200°C (for instance) for the different heating rates.

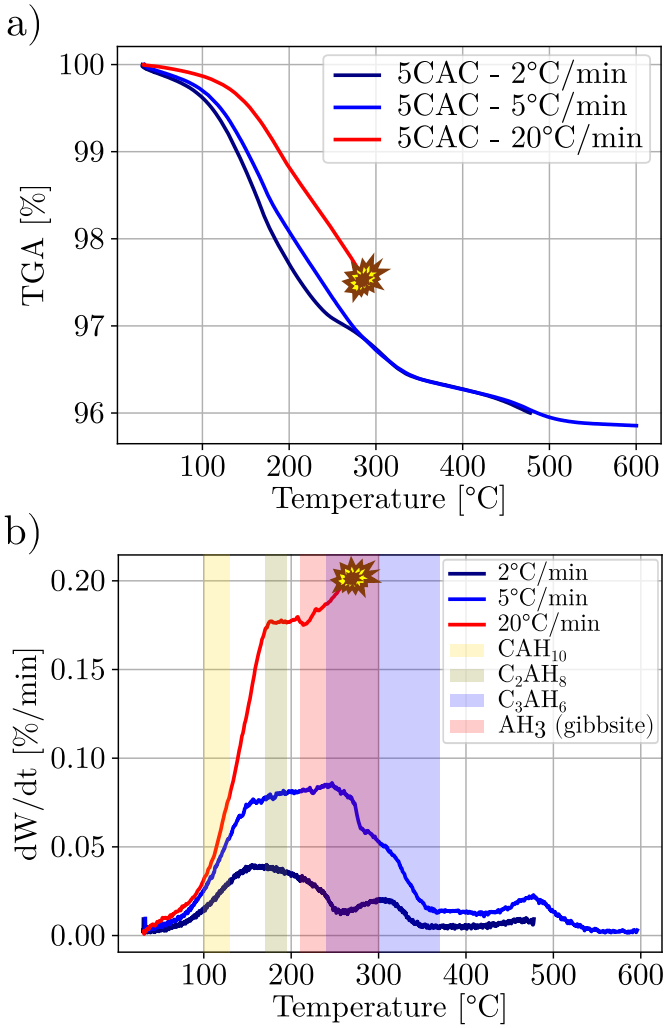

Figure 8: Thermogravimetric analysis of samples under heating rates of 2°C/min, 5°C/min and 20°C/min (a) and the mass loss derivative with respect to time (b). The colored bands marking temperature ranges indicate when specific hydrates are decomposed. The sample heated at the 20°C/min exploded during the test.

Figure 8 (b) reports the time derivative of the weight loss highlighting the ranges of hydrate decomposition. The peak observed around 140°C for the 2°C/min and 5°C/min samples only occurs at 180°C for the sample heated

at 20°C/min. This explains that dehydration reactions are shifted to higher temperatures due to the kinetic effects providing an explanation for the distinct behaviors observed for the samples as highlighted in Figure 7. A more accurate simulation of this kinetic effect would require directly measuring the temperature evolution inside the sample.

Figure 9 reports the behaviors at the bottom of the samples, which seems more similar, considering both the drying rates and their linear fits. At the bottom of the sample, the effects of the heating rate applied at the top are reduced, because the thermal energy transport is also controlled by the thermal conductivity of the material. Nonetheless, peaks in the drying rate emerge earlier and are less intense for the fast heating sample.

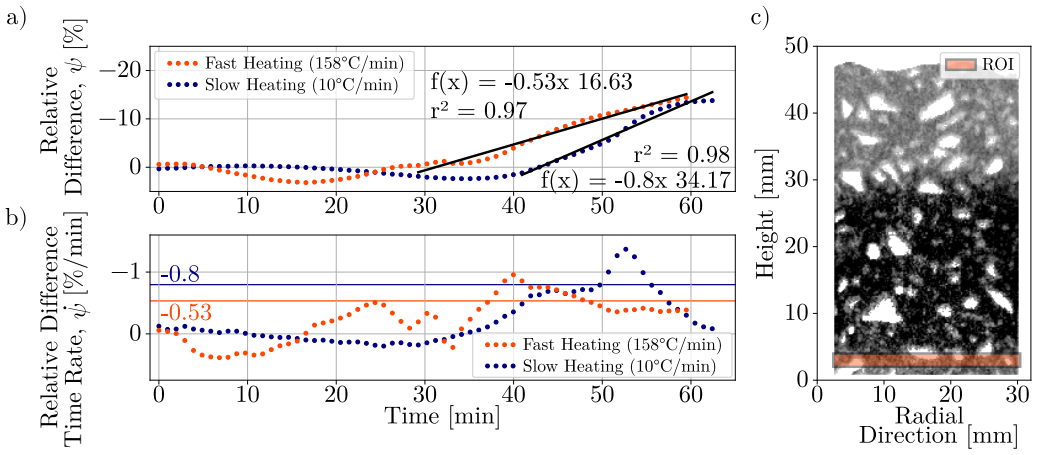

Figure 9: Relative difference evolution of a 2mm slab at the bottom of the samples (a) and the relative difference time rate (b). The axial slice presented in (c) is only to highlight the region of interest.

Besides these localized effects, the overall drying speed can be described through the fraction of the sample whose attenuation has significantly changed,

as described in Section 2 and detailed by Moreira et al. [17]. Figure 10 shows this evolution for both tests which highlights a marked difference in speed, as well as the delay between the start of the test and the inception of drying.

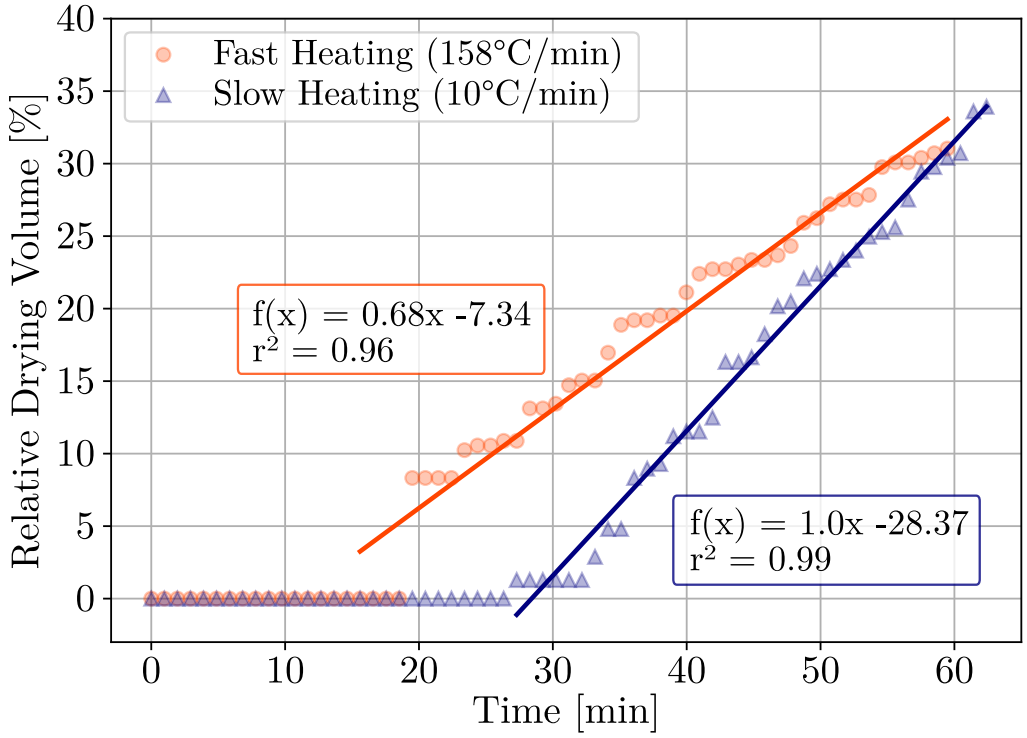

Figure 10: Relative drying volume for the fast and slow heating samples obtained through the drying front position.

It can be observed that although the moisture accumulation zone (Figures 7 and 9) and the drying front velocities (Figure 10) were notably different, the overall behavior was similar, and the only difference was the time when the drying starts. The profiles seem to be approaching each other.

This behavior could be explained by the heating conditions and position where the moisture increase is in the sample. Firstly, both heating curves

attained the same final constant temperature of 500°C. Thus, after the 48min mark, the temperatures of the heater are the same for both cases (see Figure 3). Secondly, as the moisture accumulation position inside the samples is roughly similar (as observed in Figures 4, 5 and 6), the mass transport at the latter stages of the drying is similar for both cases.

The above observations are in agreement with the results of numerical models, where the heating rate directly affects the pressurization and, as a consequence, the water distribution [33, 14, 31, 27]. Additionally, they also match the industrial experience. The moisture accumulation identified here can be directly related to the liquid water condensation observed on the cold surface of walls unidirectionally heated. The multiple occurrence of such a phenomenon was reported, ranging from industrial applications [30], where "weep holes" are commonly drilled through the steel outer shell to drain liquid water [34, 35], to experimental studies in refractories [36], as well as Portland cement structures [6, 37].

The current findings shed light on the role of the heating curves on the geometry and extent of moisture accumulation and the consequent heightened risk of explosive spalling. Nonetheless, various physical and chemical transformations occurred simultaneously during this process, which restrains the unequivocal development of guidelines and optimal procedures.

4. Conclusions

This work highlights the importance of full-field observation of the moisture distribution in porous media to understand the complex dynamics of mass transport involved in the heating of partially saturated materials. This

work adds to previous studies on Portland cement concrete and highlights how neutron tomography is a powerful tool to understand the drying behavior of refractory castables.

To the best of our knowledge, this is the first time the effect of heating rate on the drying speed and moisture accumulation ahead of the front has been directly studied. Faster heating accelerates and increases the extent of moisture accumulation and it changes the position of maximum moisture clog. The latter is believed to trigger explosive spalling. This also provides the first explanation for the well-known connection between slower heating rates and safer drying. It was also found that because the final temperature of the heater was the same, the total time (1 hour) was enough to reach similar states of water distribution for both cases

These findings move the challenge of improving the efficiency of the drying schedules towards minimizing and controlling the moisture accumulation without relying solely on over-conservative and slow heating rates.

Future studies will deploy the presented approach to analyze the effect of different additives, heating profiles and material compositions. This can provide insights into the processes and be used as a route to validate numerical models, which can additionally help to retrieve properties that cannot be directly assessed by conventional tests.

5. Acknowledgments

This study was financed in part by the Coordenação de Aperfeiçoamento de Pessoal de Nível Superior - Brasil (CAPES) - Finance Code 001. The authors would like to thank the Fundação de Amparo à Pesquisa do Estado

de São Paulo - FAPESP (grant number: 2021/00251-0). Finally, the authors are thankful for FIRE support to carry out this work and for A. P. da Luz for helping to prepare the samples.

The raw datasets collected at NeXT-Grenoble are available at: `https://doi.ill.fr/10.5291/ILL-DATA.UGA-112`

References

[1] C. R. Gagg, Cement and concrete as an engineering material: An historic appraisal and case study analysis, Engineering Failure Analysis 40 (2014) 114–140.

[2] C. Schacht, Refractories Handbook, Mechanical engineering, CRC Press, 2004. URL: https://books.google.com.br/books?id=8oI2plVDQxUC.

[3] A. P. da Luz, M. A. L. Braulio, V. C. Pandolfelli, Refractory castable engineering, Goller Verlag GmbH, Baden-Baden, 2015, pp. 331–334.

[4] A. P. Luz, M. H. Moreira, M. A. L. Braulio, C. Parr, V. C. Pandolfelli, Drying behavior of dense refractory ceramic castables. part 1–general aspects and experimental techniques used to assess water removal, Ceramics International 47 (2021) 22246–22268.

[5] Z. Ningsheng, L. Jiehua, Concepts, approaches and practices, Refractories World Forum 8 (2016) 99–110.

[6] R. Jansson, Fire spalling of concrete: theoretical and experimental studies, Ph.D. thesis, KTH Royal Institute of Technology, 2013.

[7] M. Ozawa, S. Uchida, T. Kamada, H. Morimoto, Study of mechanisms of explosive spalling in high-strength concrete at high temperatures using acoustic emission, Construction and Building Materials 37 (2012) 621–628. doi:10.1016/j.conbuildmat.2012.06.070.

[8] M. H. Moreira, S. Dal Pont, R. F. Ausas, A. P. Luz, T. M. Cunha, C. Parr, V. C. Pandolfelli, Main trends on the simulation of the drying of refractory castables-review, Ceramics International 47 (2021) 28086–28105.

[9] M. D. Innocentini, F. A. Cardoso, M. M. Akyioshi, V. C. Pandolfelli, Drying stages during the heating of high-alumina, ultra-low-cement refractory castables, Journal of the American Ceramic Society 86 (2003) 1146–1148.

[10] M. D. Innocentini, M. F. Miranda, F. A. Cardoso, V. C. Pandolfelli, Vaporization processes and pressure buildup during dewatering of dense refractory castables, Journal of the American Ceramic Society 86 (2003) 1500–1503.

[11] B. P. Bezerra, A. P. Luz, V. C. Pandolfelli, Novel drying additives and their evaluation for self-flowing refractory castables, Ceramics International 46 (2020) 3209–3217.

[12] P. Meunier, J. Mindeguia, P. Pimienta, Mass, temperature and pressure measurements during the dry out of refractory castables, in: 51st International Colloquium on Refreactories, 2008, pp. 95–98.

[13] P. Meunier, P. Ermtraud, Methods to assess the drying ability of refractory castables, in: Proceedings of the Unified International Technical Conference on Refractories (UNITECR 2013), Wiley Online Library, 2014, pp. 959–964.

[14] K. G. Fey, I. Riehl, R. Wulf, U. Gross, Experimental and numerical investigation of the first heat-up of refractory concrete, International Journal of Thermal Sciences 100 (2016) 108–125. URL: http://dx.doi.org/10.1016/j.ijthermalsci.2015.09.010. doi:10.1016/j.ijthermalsci.2015.09.010.

[15] A. J. Barakat, L. Pel, O. C. G. Adan, One-dimensional NMR imaging of high-temperature first-drying in monolithics, Applied Magnetic Resonance 49 (2018) 739–753.

[16] A. J. Barakat, L. Pel, O. Krause, O. C. Adan, Direct observation of the moisture distribution in calcium aluminate cement and hydratable alumina-bonded castables during first-drying: An NMR study, Journal of the American Ceramic Society 103 (2020) 2101–2113.

[17] M. Moreira, S. Dal Pont, A. Tengattini, A. da Luz, V. Pandolfelli, Experimental proof of moisture clog through neutron tomography in a porous medium under truly one-directional drying, Journal of the American Ceramic Society 105 (2021) 3534–3543.

[18] A. Tengattini, S. Dal Pont, H. Cheikh Sleiman, F. Kisuka, M. Briffaut, Quantification of evolving moisture profiles in concrete samples subjected to temperature gradient by means of rapid neutron tomography: Influence of boundary conditions, hygro-thermal loading history and spalling mitigation additives, Strain 56 (2020) e12371.

[19] D. Dauti, A. Tengattini, S. Dal Pont, N. Toropovs, M. Briffaut, B. Weber, Some observations on testing conditions of high-temperature ex-

periments on concrete: An insight from neutron tomography, Transport in Porous Media (2020) 1–12.

[20] D. Dauti, A. Tengattini, S. Dal Pont, N. Toropovs, M. Briffaut, B. Weber, Analysis of moisture migration in concrete at high temperature through in-situ neutron tomography, Cement and Concrete Research 111 (2018) 41–55.

[21] L. Stelzner, B. Powierza, F. Weise, T. Oesch, R. Dlugosch, B. Meng, Analysis of moisture transport in unilateral-heated dense high-strength concrete, in: 5th International Workshop on Concrete Spalling Due to Fire Exposure, 2017.

[22] T. Bintz, S. M. Nagel, L. Stelzner, R. Lauinger, W. Schmidt, S. Kruschwitz, An NMR tomograph for building materials-applications, experimental studies and limitations, in: 2021 13th International Conference on Electromagnetic Wave Interaction with Water and Moist Substances (ISEMA), IEEE, 2021, pp. 1–5.

[23] A. P. Luz, M. H. Moreira, R. Salomão, M. A. L. Braulio, V. C. Pandolfelli, Drying behavior of dense refractory castables. part 2–drying agents and design of heating schedules, Ceramics International 48 (2022) 2965–2987.

[24] A. J. Barakat, Direct observation of the moisture distribution in heated calcium alumina-and hydratable alumina-bonded castables during first-drying, using NMR imaging, Ph.D. thesis, Technische Universiteit Eindhoven (thesis) Eindhoven, 2019.

[25] R. G. Pileggi, V. C. Pandolfelli, A. E. Paiva, J. Gallo, Novel rheometer for refractory castables, American Ceramic Society Bulletin 79 (2000) 54–58.

[26] A. Tengattini, N. Lenoir, E. Andò, B. Giroud, D. Atkins, J. Beaucour, G. Viggiani, NeXT-Grenoble, the Neutron and X-ray tomograph in Grenoble, Nuclear Instruments and Methods in Physics Research Section A: Accelerators, Spectrometers, Detectors and Associated Equipment 968 (2020) 163939.

[27] D. Dauti, S. Dal Pont, M. Briffaut, B. Weber, Modeling of 3D moisture distribution in heated concrete: From continuum towards mesoscopic approach, International Journal of Heat and Mass Transfer 134 (2019) 1137–1152.

[28] R. Salomão, V. C. Pandolfelli, The particle size distribution effect on the drying efficiency of polymeric fibers containing castables, Ceramics International 34 (2008) 173–180.

[29] A. Savitzky, M. J. Golay, Smoothing and differentiation of data by simplified least squares procedures., Analytical chemistry 36 (1964) 1627–1639.

[30] G. Palmer, J. Cobos, T. Howes, The accelerated drying of refractory concrete - part 1 : A review of current understanding, Refractories Worldforum 6 (2014) 75–83.

[31] K.-G. Fey, I. Riehl, R. Wulf, U. Gross, First heat-up of 1D multi-layer walls and 2D geometries consisting of refractory con-

crete, International Journal of Thermal Sciences 116 (2017) 159–171. URL: http://linkinghub.elsevier.com/retrieve/pii/S1290072915302726. doi:10.1016/j.ijthermalsci.2016.11.021.

[32] T. N. Nguyen, D. H. Lee, J. J. Kim, Effect of electrospun nanofiber additive on selected mechanical properties of hardened cement paste, Applied Sciences 10 (2020) 7504.

[33] Z.-X. Gong, A. S. Mujumdar, Review of R&D in drying of refractories, Drying Technology 25 (2007) 1917–1925. URL: http://www.tandfonline.com/doi/abs/10.1080/07373930701727200. doi:10.1080/07373930701727200.

[34] D. Nandi, Future trends in application of monolithic refractories in the cement industry, Transactions of the Indian Ceramic Society 42 (1983) 164–168.

[35] P. Sengupta, Refractory design, installation, and maintenance, in: Refractories for the Cement Industry, Springer, 2020, pp. 99–134.

[36] R. Moore, J. Smith, T. Sander, N. Severin, Dewatering monolithic refractory castables: experimental and practical experience, in: UNITECR'97. Proc. Unified Int. Tech. Conf. on Refractories. 5 th Biennial Worldwide Congress." Refractories- A Worldwide Technology"., volume 2, 1997, pp. 573–582.

[37] M. Guerrieri, S. Fragomeni, Spalling of large-scale walls exposed to a hydrocarbon fire, Journal of Materials in Civil Engineering 31 (2019) 04019249.